


RESEARCH ARTICLE

Collision-free path planning for cable-driven continuum robot based on improved artificial potential field

Meng Ding, Xianjie Zheng, Liaoxue Liu, Jian Guo and Yu Guo 

School of Automation, Nanjing University of Science and Technology, Nanjing China

Corresponding author: Yu Guo; Email: guoyu@njust.edu.cn

Received: 26 September 2023; **Revised:** 14 December 2023; **Accepted:** 8 January 2024; **First published online:** 5 March 2024

Keywords: continuum robot; collision-free path planning; artificial potential field; beetle antennae search

Abstract

Continuum robot has become a research hotspot due to its excellent dexterity, flexibility and applicability to constrained environments. However, the effective, secure and accurate path planning for the continuum robot remains a challenging issue, for that it is difficult to choose a suitable inverse kinematics solution due to its redundancy in the confined environment. This paper presents a collision-free path planning method based on the improved artificial potential field (APF) for the cable-driven continuum robot, in which the beetle antennae search algorithm is adopted to deal with the optimal problem of APF without the necessary for velocity kinematics. In addition, the local optimum problem of traditional APF is solved by the randomness of the antennae's direction vector which can make the algorithm easily jump out of local minima. The simulation and experimental results verify the efficiency of the proposed path planning method.

1. Introduction

Inspired by the bionics, various configurations of continuum robots have emerged in recent years. Compared with traditional rigid robots, continuum robots with elastic structure and infinite/redundant degrees of freedom provide continuous bending capabilities and exhibit strong dexterity in narrow and unstructured environments [1–4]. Due to their superior performance in constrained environments, the continuum robots have received widespread attention and applied in various fields such as nuclear equipment maintenance [5, 6], medical surgery [7, 8], rehabilitation nursing [9], space on-orbit service [10, 11] and so forth. However, the path planning problem remains complex and deserves further research for this highly nonlinear and coupled system.

The path planning problem is to generate a feasible trajectory that avoids obstacles and satisfies the physical constraints of the robot system, which is a prerequisite for the continuum robot to successfully complete tasks. Meanwhile, it is well known that the mapping between the configuration space and work space of continuum robot is highly complicated. Several scholars have conducted researches on the collision-free path planning for the continuum robot and related strategies have been addressed, such as Jacobian-based method [12], rapidly-exploring random trees (RRT) [13], optimization method [14–16], intelligent learning [17, 18], curve simulation method [19], APF [20–22], follow the leader (FTL) [23, 24] and other methods [25–27]. Memar et al. [12] proposed an improved Jacobian-based motion planning method based on the constant curvature model. Meng et al. [13] put forward an RRT* path planner with a Jacobian-based approach for workspace searching. Y Tian et al. [22] presented an improved APF algorithm for overall configuration planning of the hyper-redundant manipulator by constructing a virtual guiding pipeline. However, most of the above researches for continuum robot are based on velocity kinematics. The Jacobian inverse solution may not only generate singular values but also lead to higher computational complexity with more segments of robot. J Lai et al. [14] computed

the inverse kinematics by solving a damped least-square optimization problem for the task of tip trajectory tracking under constrained conditions. T Ning et al. [18] presented a data-driven model-free motion control strategy based on continuous-time zeroing neural network, which shows superior performance in terms of accuracy. However, the scheme only utilizes the end-effector position feedback for trajectory tracking, which ignoring the attitude of the continuum robot. Mohammad et al. [23] adopted a FTL strategy that enables the snake-like robot to move along the path guided by the tip-led paths. Nevertheless, more stringent constraints on the shape and tip of the robot are necessary for the complex path planning, resulting in higher computational and control complexity. G Niu et al. [15] proposed an optimization method based on region clipping which searches forward in the configuration space for collision-free path planning. However, the optimization method was just suitable for some specific environments with poor scalability.

Considering that APF has high planning efficiency and environmental adaptability [28, 29], if the path planning task can be completed through forward searching in the configuration space, complex inverse solution and singular value problems in existing researches can be reasonably solved. However, the configuration space potential field method has certain limitations in planning and obstacle avoidance for robots with multiple degrees of freedom, as it is difficult to obtain a complete representation of the obstacle space. In order to satisfy the path planning through forward kinematics and avoid the local minima existing in traditional APF, this paper addresses an improved APF method combined with the beetle antennae search algorithm called BAS-APF for collision-free path planning of continuum robot. The BAS algorithm is a recently emerged metaheuristic algorithm inspired by detecting and searching behavior of beetles [30, 31], which has been well applied in some practical scenarios, i.e., motion planning, tracking control or trajectory optimization of robot [32–34], optimization of neural network model [35], rolling bearing fault diagnosis [36] and acoustic signal analysis [37].

In this paper, the BAS-APF method is presented for collision-free path planning of the cable-driven continuum robot, which focuses on adopting the BAS algorithm to determine the attitude angles guided by the decreasing potential field. The main contributions are included as follows:

1. The proposed BAS-APF algorithm can be applied for target path planning and obstacle avoidance simultaneously, along with an accompanying collision detection model designed for the specific configuration of the continuum robot.
2. The proposed algorithm is a position-level forward search method in the configuration space. The approach avoids calculating Jacobian matrix inverse unlike most velocity-level strategies and thus reduces the computation cost.
3. The local optimum problem of APF is solved by utilizing the randomness of the antennae's direction vector searching in the configuration space.

The remainder of this paper is outlined as follows. The kinematics model and collision detection model are established in Section 2. Section 3 introduces the BAS-APF algorithm for the collision-free path planning in detail. In Section 4, the path planning method is verified by the simulation and experiments. Section 5 provides conclusion of this paper and future prospects.

2. Problem formulation

2.1. Problem description

The continuum robot is generally composed of several segments and each segment is driven by four cables [38]. The spring deforms elastically by pulling the actuated cables, resulting in flexible bending of the robot. The spacer disks are evenly spaced and the adjacent spacer disks are connected by universal joints. Figure 1 shows a two-segment cable-driven continuum robot prototype model.

The goal of path planning for the continuum robot is that a continuous path needs to be found between the initial state and the target state in the constrained workspace. Figure 2 shows the operation of a two-segment continuum robot in the task space with three obstacles from the starting point 'S' to the end

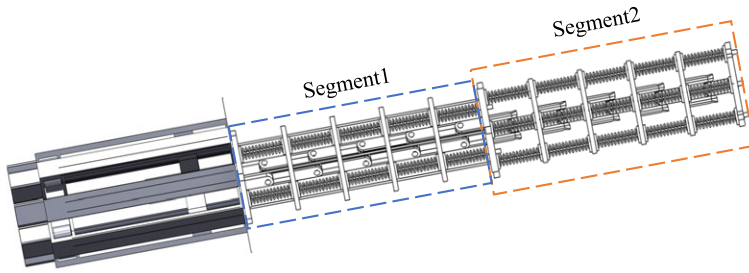


Figure 1. A two-segment cable-driven continuum robot prototype.

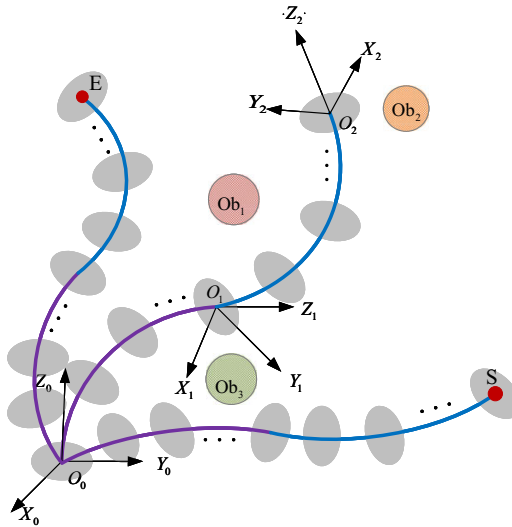


Figure 2. Continuum robot path planning in the obstacle environment.

target point ‘E’. The Cartesian coordinate $O_1 - X_1Y_1Z_1$ is the base coordinate frame of the continuum robot system. $O_2 - X_2Y_2Z_2$ and $O_3 - X_3Y_3Z_3$ represent the coordinate frame of the end the spacer disk for the first-segment and second-segment continuum robot respectively. This work aims to find a feasible path that avoids obstacles and satisfies the physical constraints of the continuum robot while considering the efficiency and accuracy in performing tasks.

2.2. Kinematic model

The kinematics model of the N -segment continuum robot model is established in this section. Due to the small spacing between adjacent disks, the elastic deformation produced by springs with the same specifications under the approximate force is also approximately equal. Thus, it is assumed that each segment of the continuum robot acts like a constant curvature arc. For the i th-segment, the coordinate frame schematic is illustrated in Fig. 3 (a). Each segment of the continuum robot can be parameterized by two variables β_i and γ_i in the configuration space, where β_i represents the bending angle and γ_i is rotation angle around the axis Z_{i-1} respectively. The arc length of the i th-segment is denoted by L_i . Based on the assumption of constant curvature, the bending angles of the adjacent spacer disks in the same segment are equal. As shown in Fig. 3 (b), the bending angle of j th adjacent spacer disk is defined as β_{ij}

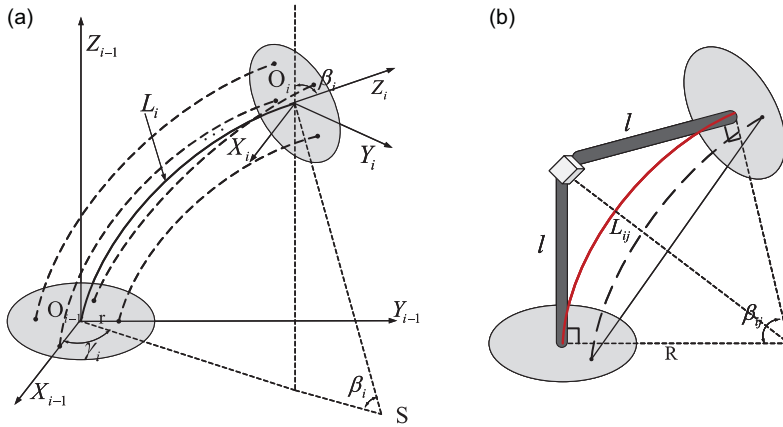


Figure 3. (a) Coordinate frame schematic of the *i*th-segment continuum robot and (b) bending schematic of the adjacent spacer plates.

and the distance between them is $2l$. According to the geometric relationship, the arc length L_{ij} can be calculated by

$$L_{ij} = \beta_{ij}R \tag{1}$$

where R is the arc radius. In addition, it is easy to obtain the relationship between R and l .

$$l = R \tan\left(\frac{\beta_{ij}}{2}\right) \tag{2}$$

Thus, the arc length L_i is given by

$$L_i = k\beta_{ij}R = \frac{k\beta_{ij}l}{\tan\left(\frac{\beta_{ij}}{2}\right)} = \frac{\beta_j l}{\tan\left(\frac{\beta_j}{2k}\right)} \tag{3}$$

where k is the number of the spacer disks in the *i*th-segment.

The transformation matrix for the *i*th-segment is presented as [39]

$${}^{i-1}\mathbf{T}_i = \begin{pmatrix} c^2\gamma_i c\beta_i + s^2\gamma_i & c\gamma_i s\gamma_i(c\beta_i - 1) & c\gamma_i s\beta_i & \frac{L_i}{\beta_i} c\gamma_i(1 - c\beta_i) \\ c\gamma_i s\gamma_i(c\gamma_i - 1) & c^2\gamma_i + s^2\gamma_i c\beta_i & s\gamma_i s\beta_i & \frac{L_i}{\beta_i} s\gamma_i(1 - c\beta_i) \\ -c\gamma_i s\beta_i & -s\gamma_i s\beta_i & c\beta_i & \frac{L_i}{\beta_i} s\beta_i \\ 0 & 0 & 0 & 1 \end{pmatrix} \tag{4}$$

where $c\beta_i, c\gamma_i, s\beta_i, s\gamma_i$ stand for the abbreviation of function $\cos \beta_i, \cos \gamma_i, \sin \beta_i, \sin \gamma_i$ respectively.

The kinematic mapping relationship for the N -segment continuum robot can be expressed as

$${}^0\mathbf{T}_N = {}^0\mathbf{T}_1 \cdot {}^1\mathbf{T}_2 \cdot \dots \cdot {}^{N-1}\mathbf{T}_N \tag{5}$$

Since the actuated cables remain taut between the spacers as seen from Fig. 3 (b), the length variation of the actuated cables $\Delta l_{i,m} (m = 1, 2, 3, 4)$ can be expressed as

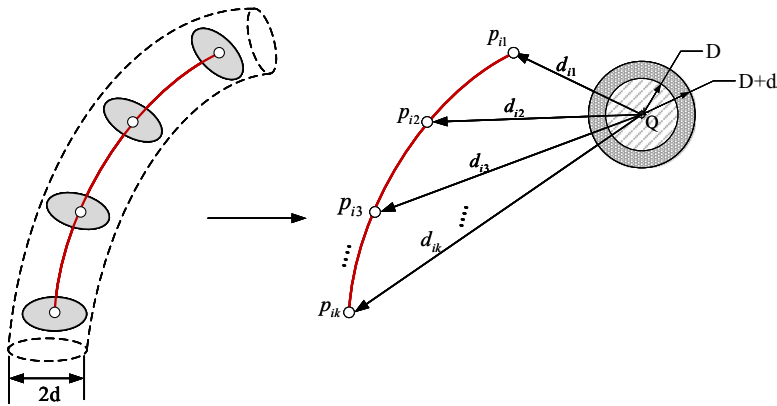


Figure 4. Collision detection model.

$$\begin{aligned}
 \Delta l_{i,1} &= \sum_{n=1}^i L_i - 2k \left(\frac{l}{\tan\left(\frac{\beta_i}{2k}\right)} - r \cos\left(\gamma_n + (k-1)\frac{\pi}{2N}\right) \right) \sin\left(\frac{\beta_i}{2k}\right) \\
 \Delta l_{i,2} &= \sum_{n=1}^i L_i - 2k \left(\frac{l}{\tan\left(\frac{\beta_i}{2k}\right)} - r \cos\left(\gamma_n + (k-1)\frac{\pi}{2N} + \frac{\pi}{2}\right) \right) \sin\left(\frac{\beta_i}{2k}\right) \\
 \Delta l_{i,3} &= \sum_{n=1}^i L_i - 2k \left(\frac{l}{\tan\left(\frac{\beta_i}{2k}\right)} + r \cos\left(\gamma_n + (k-1)\frac{\pi}{2N}\right) \right) \sin\left(\frac{\beta_i}{2k}\right) \\
 \Delta l_{i,4} &= \sum_{n=1}^i L_i - 2k \left(\frac{l}{\tan\left(\frac{\beta_i}{2k}\right)} + r \cos\left(\gamma_n + (k-1)\frac{\pi}{2N} + \frac{\pi}{2}\right) \right) \sin\left(\frac{\beta_i}{2k}\right)
 \end{aligned} \tag{6}$$

Where r is the distance between the cable hole and center hole on the spacer disks.

Remark 1. As shown in Eq. (4), there exists a singular problem when β_i is equal to 0. Thus, the fifth-order Taylor expansions of $\cos \beta_i$ and $\sin \beta_i$ with respect to β_i are applied to avoid singularities, shown as follows:

$$\begin{aligned}
 \sin \beta_i &= \beta_i - \frac{\beta_i^3}{3!} + \frac{\beta_i^5}{5!} \\
 \cos \beta_i &= 1 - \frac{\beta_i^2}{2!} + \frac{\beta_i^4}{4!}
 \end{aligned} \tag{7}$$

2.3. Collision detection

For the collision detection techniques of the traditional rigid link manipulators, the links are generally equivalent to cylinders, and the minimum distance between the central axis and the obstacle needs to be measured to determine whether the manipulator collides with the obstacle [40]. Since the bending direction of the cable-driven continuum robot is not always fixed during the movement and the spacer disks increase the radial distance of the robot body, the robot cannot be simply regarded as an arc in collision detection.

Inspired by the collision detection technique of the rigid link manipulators, each segment of the continuum robot is simplified with a curved tubular model in Fig. 4. In order to further simplify the collision detection model, the radial radius of the tubular model is superimposed on the obstacle ball bounding box, where D represents the radius of the ball bounding box and d is the radius of the tubular model. Then the center points $p_{ij}(j = 1, 2, \dots, k)$ of the spacer disks of the i th-segment are defined as

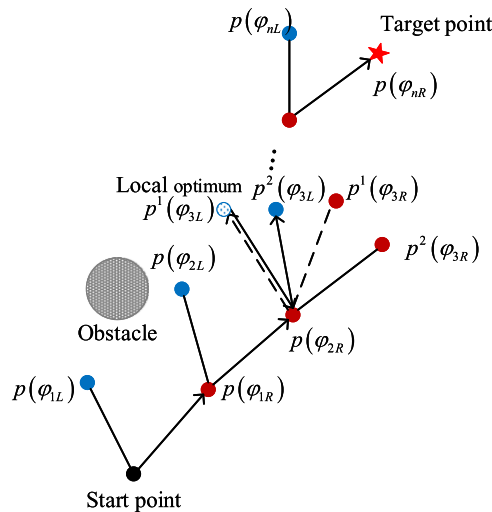


Figure 5. The path planning process of the BAS-APF algorithm.

control points which are used to measure the distances $d_{ij}(j = 1, 2, \dots, k)$ between them and the center of obstacle Q. The minimum distance from the obstacle for the i th-segment d_i can be expressed as

$$d_i = \min\{d_{ij}\}, j = 1, 2, \dots, k \tag{8}$$

Therefore, if the minimum distance $d_i(i = 1, 2 \dots, N)$ satisfies $d_i > D + d$, it can be considered that the continuum robot will not collide with the obstacle.

3. Path planning algorithm for obstacle avoidance

In this section, we will formulate the proposed BAS-APF algorithm for the collision-free path planning. The beetle searches in the configuration space with both antennae as the searching direction to realize the path planning based on APF, which avoids the complex inverse kinematics calculation.

3.1. BAS-APF algorithm

As is shown in Eq. (9), the basic concept of path planning based on APF is to construct a virtual potential field U in the motion space of the robot, where the attraction potential field U_{att} attracts the robot to move toward the target position and the repulsion potential field U_{rep} excludes the robot from obstacles.

$$U = U_{att} + U_{rep} \tag{9}$$

Gradient descent method is usually used to deal with the optimization problem shown in Eq. (9), so as to obtain the joint angle of the robot under the global minimum potential field U_{min} . However, for the case that the working environment of robot is complicated, the drawback that restricts the gradient descent algorithm is the possible existence of local minima in the potential field, where the attraction and repulsion forces are equal in magnitude and opposite in direction.

BAS algorithm imitates the foraging behavior of beetle, using its antennae to search and turn to the direction with stronger smell. The beetle measures the odor concentration at each step to obtain the direction of the next step until it reaches the endpoint, instead of moving randomly in any direction. Inspired by the biological behavior, APF method can be combined with BAS algorithm to handle the problem of local optimization. Figure 5 shows the process of obstacle avoidance path planning based on BAS-APF algorithm, where specially presents how to avoid local optimum.

This paper constructs a potential field model in the task space and the potential field functions are given considering the special configuration of the continuum robot. The attraction potential field is expressed as

$$U_{att} = \begin{cases} k_a \cdot \|P(\varphi) - P_{ta}\|^2, & \|P(\varphi) - P_{ta}\| \leq d_{att} \\ k_a \cdot \|P(\varphi) - P_{ta}\|, & \|P(\varphi) - P_{ta}\| > d_{att} \end{cases} \tag{10}$$

where $\varphi = [\beta_1, \gamma_1, \beta_2, \gamma_2, \dots, \beta_N, \gamma_N]^T$ is defined as the attitude angle vector of the N -segment continuum robot, k_a is the attractive proportional gain, $P(\varphi)$ represents the current position of the end-effector, P_{ta} represents the target position, $\|P(\varphi) - P_{ta}\|$ represents the Euclidean distance between the two points, d_{att} is the set distance threshold.

The repulsion potential field is expressed as

$$U_{rep}(i) = \begin{cases} \infty & \|P_i(\varphi) - P_Q\| \leq D + d \\ k_r \left(\frac{1}{\|P_i(\varphi) - P_Q\|} - \frac{1}{d_o} \right) D + d & D + d < \|P_i(\varphi) - P_Q\| \leq d_o \\ 0 & \|P_i(\varphi) - P_Q\| > d_o \end{cases} \tag{11}$$

$$U_{rep} = \sum_{i=1}^K U_{rep}(i) \tag{12}$$

where k_r is the repulsive proportional gain, $P_i(\varphi)$ represents the position of the i th spacer disk, P_Q represents the position of the center of obstacle Q, $\|P_i(\varphi) - P_Q\|$ represents the Euclidean distance between the two points, d_o is the influence range of the repulsion potential field, the total number of the spacer disks K is calculated as $K = N \cdot k$.

For the cable-driven continuum robot, the computational complexity of the inverse kinematics increases rapidly as the number of segments increase. Meanwhile, the existence of multiple inverse solutions may cause the discontinuity of the planned attitude angle. In this paper, the proposed BAS-APF method mainly uses BAS algorithm to search in the configuration space until the corresponding attitude angle under the minimum potential field is found. Algorithm 1 shows the pseudocode for collision-free path planning. The main flow of path planning for continuum robot is introduced as follows:

1. The attitudes of both directions for the searching antennae at time step t can be presented as

$$\begin{cases} \varphi_t^L = \varphi_t + \lambda_t \vec{b} \\ \varphi_t^R = \varphi_t - \lambda_t \vec{b} \end{cases} \tag{13}$$

$$\vec{b} = \frac{\text{rnd}(2N, 1)}{\|\text{rnd}(2N, 1)\|} \tag{14}$$

where φ_t^L and φ_t^R denote the attitude positions of left and right antennae in the searching area respectively, φ_t denotes the attitude angle vector at time step t , λ_t is the exploration step size of the antenna, \vec{b} is a normalized random direction vector.

2. Calculate the minimum distance between each segment and obstacles, and then conduct collision detection with Eq. (8). Considering the constraint of obstacles and limitation of attitude angle, the constraint function of attitude angle $\Lambda(\varphi_t^x)$ can be defined as

$$\Lambda(\varphi_t^x) = \begin{cases} \max\{\varphi_{min}, \min\{\varphi_t^x, \varphi_{max}\}\} & \text{if } d_i > D + d \\ \varphi_t & \text{if } d_i \leq D + d \end{cases} \tag{15}$$

$i = 1, 2, \dots, N$

where $x \in \{L, R\}$, φ_{min} and φ_{max} are the lower and upper attitude angle limits respectively.

Algorithm 1. BAS-APF algorithm – collision-free path planning

Input: $\mathbf{T}_0^N, \mathbf{P}_{ta}, \mathbf{P}_Q, \mathbf{U}, N, k, D, d, k_a, k_r, d_{att}, d_0, \lambda_0, a_1, a_2, t_{end}, r_{th}$
Output: An optimal attitude angle vector $\boldsymbol{\varphi}_{best} = [\varphi_0 \varphi_1 \cdots \varphi_{t_{end}}]$

- 1: $\boldsymbol{\varphi}_0 \leftarrow$ the initial attitude angle vector
- 2: $t \leftarrow 0$
- 3: $t_{max} \leftarrow$ maximum number of iterations
- 4: **while** $t < 2 * t_{max}$ **do**
- 5: Generate normalized random direction vector \vec{b}
- 6: Calculate the both directions $\boldsymbol{\varphi}_t^L$ and $\boldsymbol{\varphi}_t^R$
- 7: Collision detection $d_i = \min\{d_{ij}\}$
- 8: Constraint attitude angle $\bar{\boldsymbol{\varphi}}_t^x (x \in \{L, R\}) \leftarrow \Lambda(\boldsymbol{\varphi}_t^x)$
- 9: Current potential fields $U(\bar{\boldsymbol{\varphi}}_t^x) \leftarrow \bar{\boldsymbol{\varphi}}_t^x (x \in \{L, R\})$
- 10: **if** $U(\bar{\boldsymbol{\varphi}}_t^x) < U(\boldsymbol{\varphi}_t)$ **then**
- 11: $\boldsymbol{\varphi}_{t+1} = \bar{\boldsymbol{\varphi}}_t^x$
- 12: **else**
- 13: $\boldsymbol{\varphi}_{t+1} = \boldsymbol{\varphi}_t$
- 14: **end if**
- 15: Move to new direction $\boldsymbol{\varphi}_{t+1}$
- 16: $t \leftarrow t + 1$
- 17: **if** $t = t_{max}$ and $\|\mathbf{P}(\boldsymbol{\varphi}_{t_{max}}) - \mathbf{P}_{ta}\| > r_{th}$ **then**
- 18: Move to previous direction $\boldsymbol{\varphi}_{t_{max}-1}$
- 19: **end if**
- 20: **end while**
- 21: Output $\boldsymbol{\varphi}_{best}$

3. The constraint attitude angle is recorded as $\bar{\boldsymbol{\varphi}}_t^x (x \in \{L, R\})$ according to the constraint function (15). Then the potential fields $U(\bar{\boldsymbol{\varphi}}_t^x)$ at the positions of the current antenna are calculated combined with Eqs. (9)–(12).
4. Update the next moving direction of the beetle along the descending direction of the potential field, the update rule is given as

$$\bar{\boldsymbol{\varphi}}_t^x = \Lambda\left(\boldsymbol{\varphi}_t - \delta_t \vec{b} \text{sgn}\left(U(\bar{\boldsymbol{\varphi}}_t^L) - U(\bar{\boldsymbol{\varphi}}_t^R)\right)\right) \tag{16}$$

Where $\bar{\boldsymbol{\varphi}}_t^x$ is the updated attitude angle, δ_t donates the updating step size of the antenna, $\text{sgn}(\cdot)$ donates the signum function.

5. Calculate the potential field $U(\bar{\boldsymbol{\varphi}}_t^x)$ at the position of the updated attitude angle and compared it with the potential field $U(\boldsymbol{\varphi}_t)$ at time step t . If the updated potential field is smaller than that at time step t , the antenna will transfer to the new position. Otherwise, it will remain in the previous position. The attitude angle for the searching antennae at time step $t + 1$ is shown as

$$\boldsymbol{\varphi}_{t+1} = \begin{cases} \bar{\boldsymbol{\varphi}}_t^x & \text{if } U(\bar{\boldsymbol{\varphi}}_t^x) < U(\boldsymbol{\varphi}_t) \\ \boldsymbol{\varphi}_t & \text{if } U(\bar{\boldsymbol{\varphi}}_t^x) \geq U(\boldsymbol{\varphi}_t) \end{cases} \tag{17}$$

6. After moving to the new position, return to step 1 and enter the next searching cycle until reaching the neighborhood range r_{th} of target point. If the cycle ends at time step t_{max} and the target position has not been reached, the beetle is considered to be trapped in the local optimum. Then turn back to the previous position at time step t_{max-1} and reenter to Step 1 for a new searching cycle.

The step size of λ_i and δ_i should be chosen based on the task requirements of the system for that the step size should be taken large when the continuum robot is far from the target point to better improve

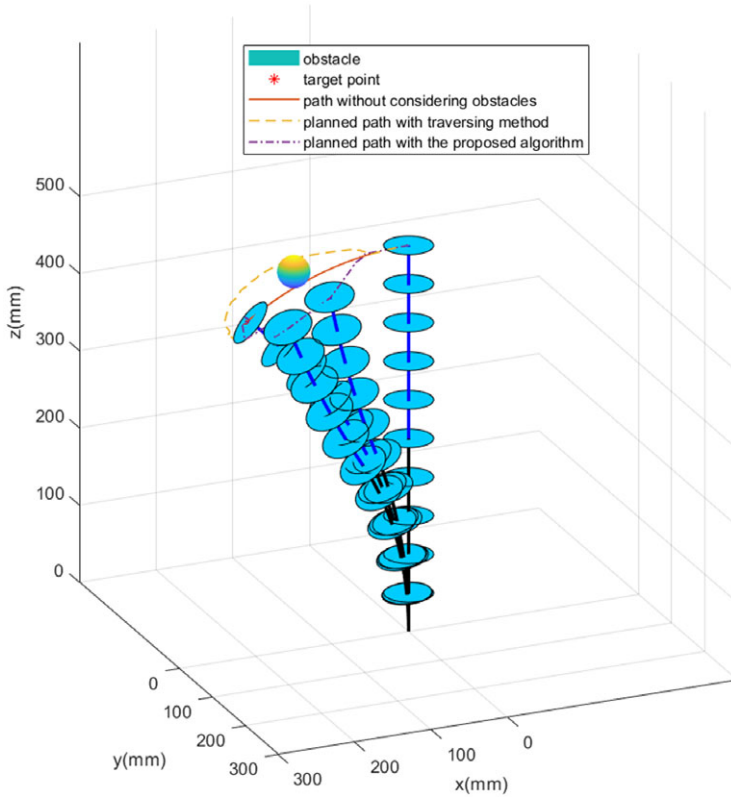


Figure 6. Path planning in the single obstacle environment.

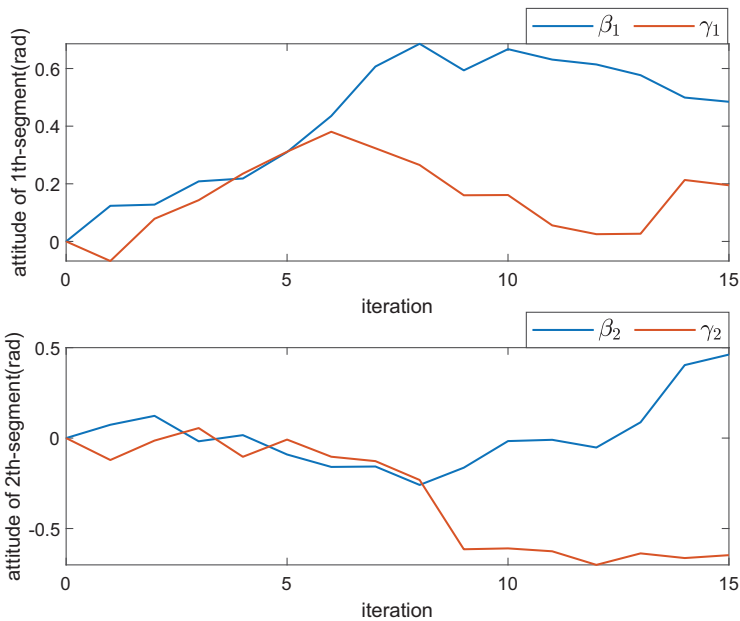


Figure 7. Attitude angle curve for the obstacle avoidance planning.

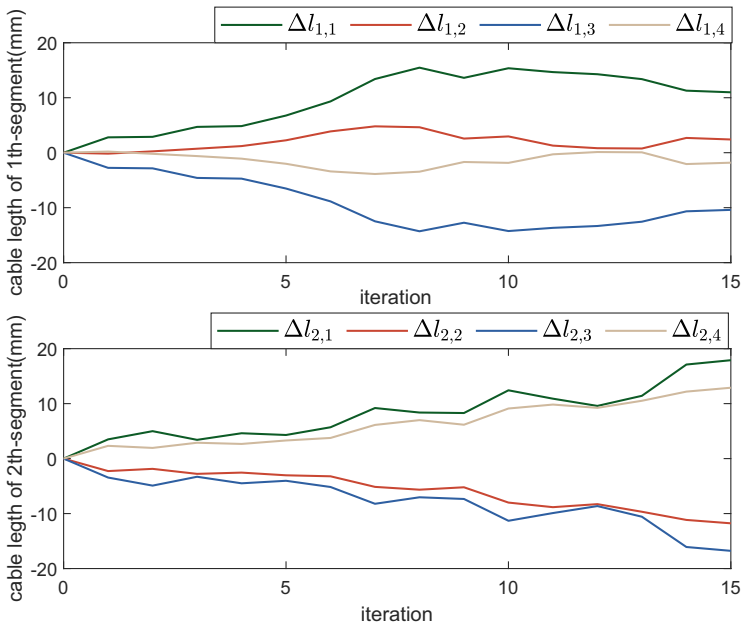


Figure 8. The length variation of the actuated cables for the obstacle avoidance planning.

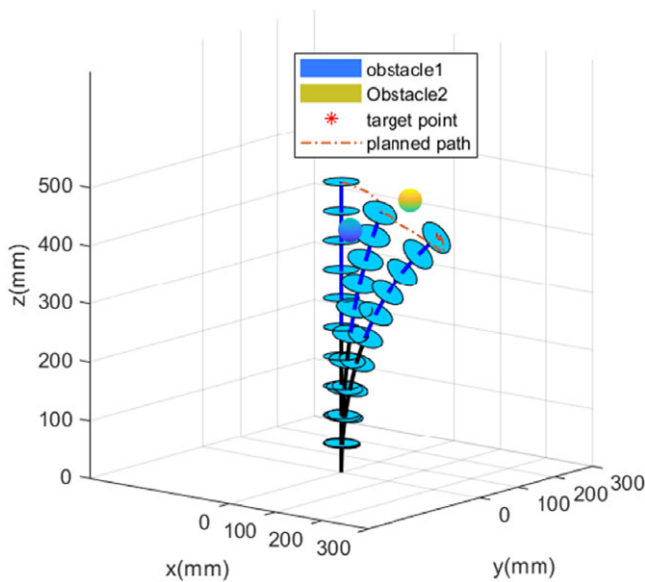


Figure 9. Path planning in the multi-obstacles environment.

the speed of path generation, and meanwhile, the small step size should be set to improve the planning accuracy when reaching near the target point. According to engineering experience, the decay function for step size can be designed as

$$\lambda_t = \lambda_0 e^{-\frac{a_1}{\|P(\varphi) - P_{ta}(\varphi)\|}} \tag{18}$$

$$\delta_t = a_2 \lambda_t \tag{19}$$

where λ_0 , a_1 and a_2 are normal numbers.

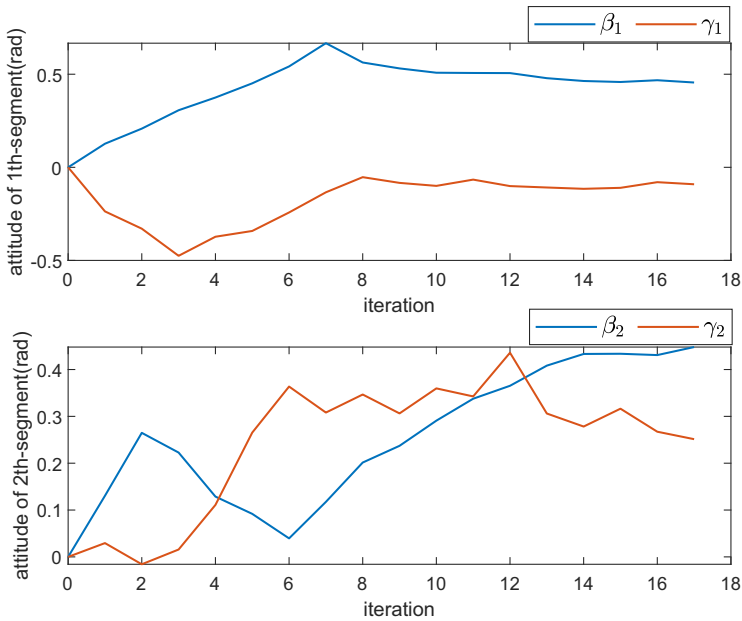


Figure 10. Attitude angle curve for the obstacle avoidance planning.

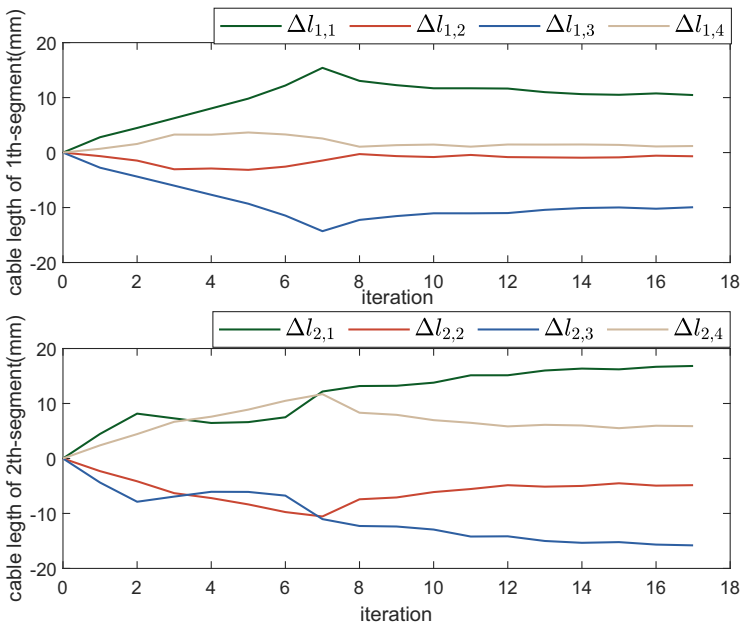


Figure 11. The length variation of the actuated cables for the obstacle avoidance planning.

Remark 2. It is noteworthy that the choice of the parameter λ_0 should refer to the distance between the obstacles and the initial point of the continuum robot in the known environment. If the distance between them is very close, the parameter should be set relatively small to avoid the robot ignoring the planning process that may collide with the obstacle.

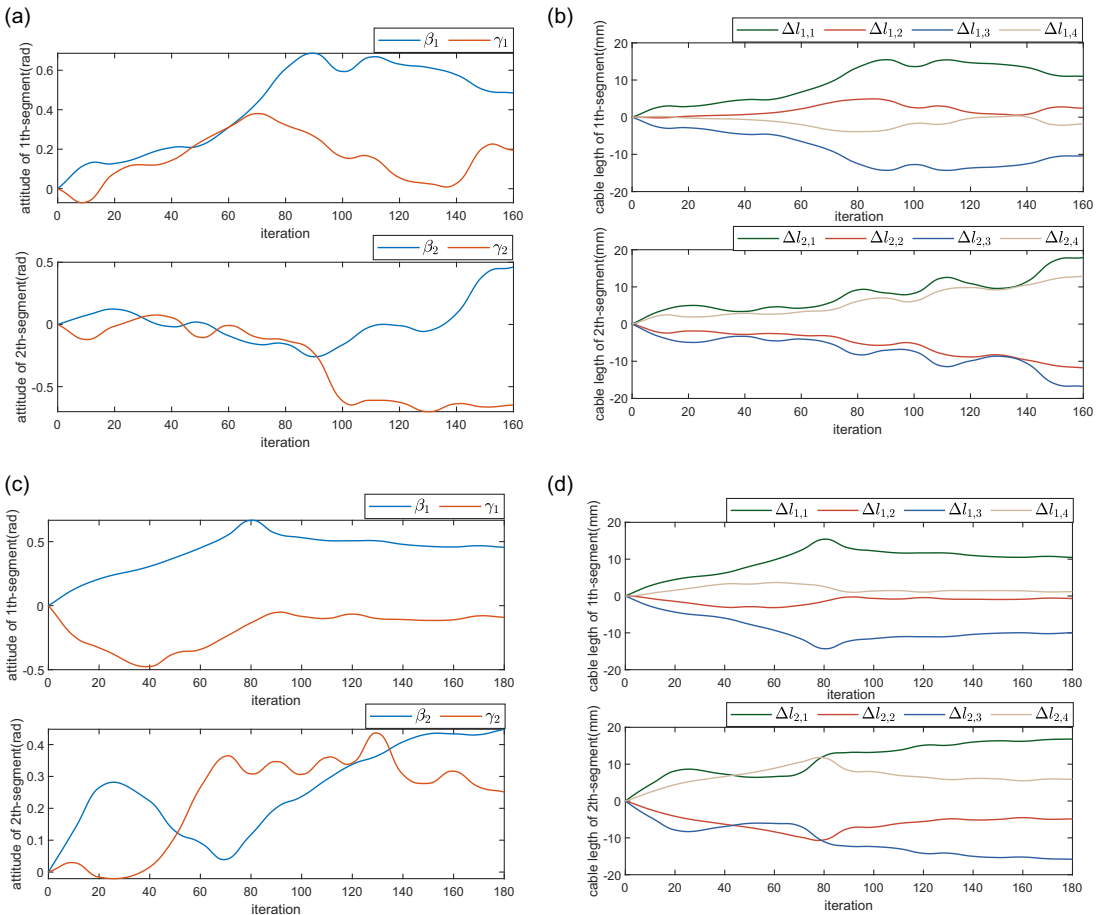


Figure 12. Curves of attitude angle and cable length after interpolation processing.

Remark 3. Since the proposed BSA-APF algorithm involves iterative processes for searching feasible paths while considering obstacle constraints, it has a time computational complexity of $O(k * M * N)$ per iteration for the N -segment continuum robot, where M is the number of the obstacles.

4. Simulation and experiment results

The simulations and experiments of collision-free path planning for two-segment continuum robot in single obstacle and multi-obstacles environment are conducted to evaluate the performance of the proposed BAS-APF algorithm in this section.

4.1. Simulation

The proposed BAS-APF algorithm is firstly applied to path planning in the single obstacle environment. Assume that the initial attitude angle of the continuum robot is $\varphi_0 = [0, 0, 0, 0]^T$ rad, the center of the obstacle is set as $P_Q = [150, 0, 490]$ mm, the radius of the obstacle is 20 mm, the target point position is set as $P_{ta} = [207.96, 0, 431.75]$ mm. The other parameters for the simulation are $d = 30$ mm, $d_0 = 60$ mm, $k = 5$, $k_a = 10$, $k_r = 1$, $a_1 = 10$, $a_2 = 1$, r_{th} .

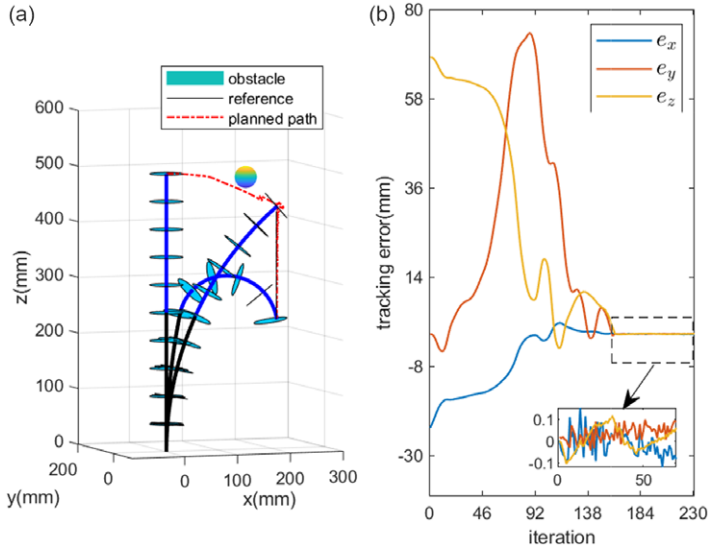


Figure 13. Trajectory tracking for two-segment continuum robot.

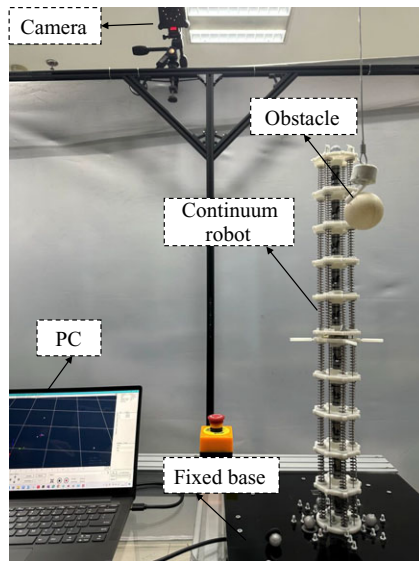


Figure 14. Two-segment cable-driven continuum robot prototype.

Figure 6 shows the comparative performance of the motion path to avoid a single obstacle. It can be seen that although the APF method based on traversing approach can avoid the obstacle well and reach the target position for the continuum robot, it needs to perform more iterations for the planning task and the planned path is much longer than that with the proposed BAS-APF method. Figures 7 and 8 show the attitude angle and cable length of each segment under the proposed algorithm respectively.

For the path planning in the two obstacles environment, the centers of the obstacles are set as $P_{Q1} = [150, 0, 490]$ mm and $P_{Q2} = [100, -100, 450]$ mm, respectively. The values of other parameters are the same as the above simulation. The motion path of the continuum robot to avoid two obstacles is shown in Fig. 9. The corresponding planned attitude angle and cable length of each segment are shown in Figs. 10 and 11.

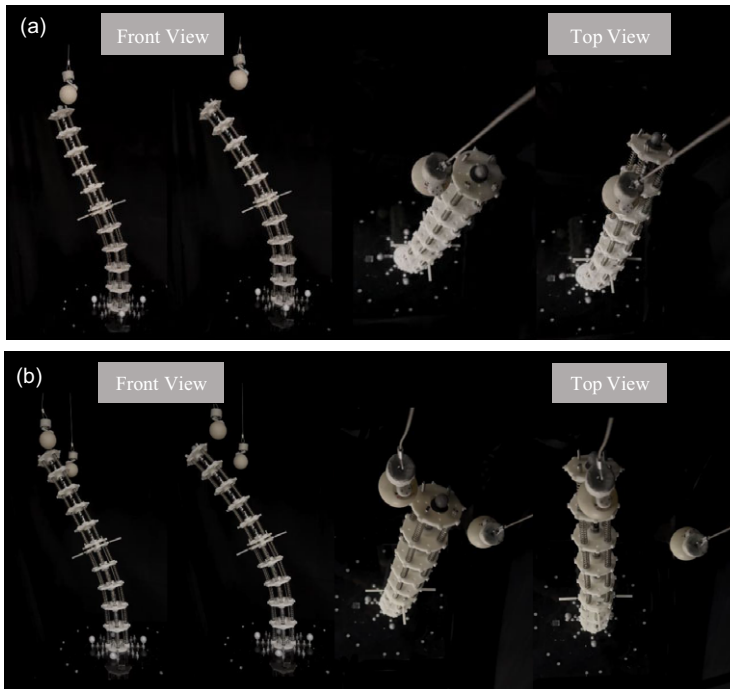


Figure 15. (a) Moving process in the single obstacle environment and (b) moving process in the multi-obstacles environment.

From the above simulations, we can see that the proposed BAS-APF method shows good performance for the path planning in single obstacle and multi-obstacles environments, especially in terms of the fast planning speed, which benefits from the design of searching variable step size. It is worth pointing out that the changes of attitude angle and cable length are discontinuous during iterations, which is not suitable for the actual system. However, this paper only discusses the path planning in the task space, while the planning method of configuration space can be combined to make the attitude angle smoother in the subsequent practical application. Here, we chose the quintic spline to interpolate attitude angles [41], where the spline function is defined piecewise on each adjacent attitude angle interval and shown as:

$$S_i(\theta) = a_i + b_i(\theta - k_i)^2 + c_i(\theta - k_i)^3 + d_i(\theta - k_i)^4 + e_i(\theta - k_i)^5 \tag{20}$$

where θ represents the attitude variable, k_i is attitude note of the spline, a_i, b_i, c_i, d_i and e_i are constant coefficients. Thus, the curves of attitude angle and cable length after interpolation processing are shown in Fig. 12.

To evaluate the performance of the proposed algorithm regarding trajectory tracking, the continuum robot was tasked with tracking a straight-line trajectory utilizing the following parametric equation:

$$\mathbf{x}_r = \mathbf{P}_{ta} + [0 \ 0 \ -2.85t]^T \tag{21}$$

where $\mathbf{P}_{ta} = [207.96, 0, 431.75]$ is the initial point of the straight-line, $t \in [0, 70]$ donates the number of iterations.

Figure 13 (a) illustrates the motion of the robot end-effector along the straight-line trajectory. Initially, the continuum robot needs to move from its starting configuration to the starting position of the reference trajectory, while avoiding obstacles. Upon reaching the starting position, the robot tracks the reference trajectory precisely. Figure 13 (b) displays the tracking error of the end-effector after interpolation and the error remains within the range of $[-0.2, 0.2]$ mm while moving along the straight-line trajectory.

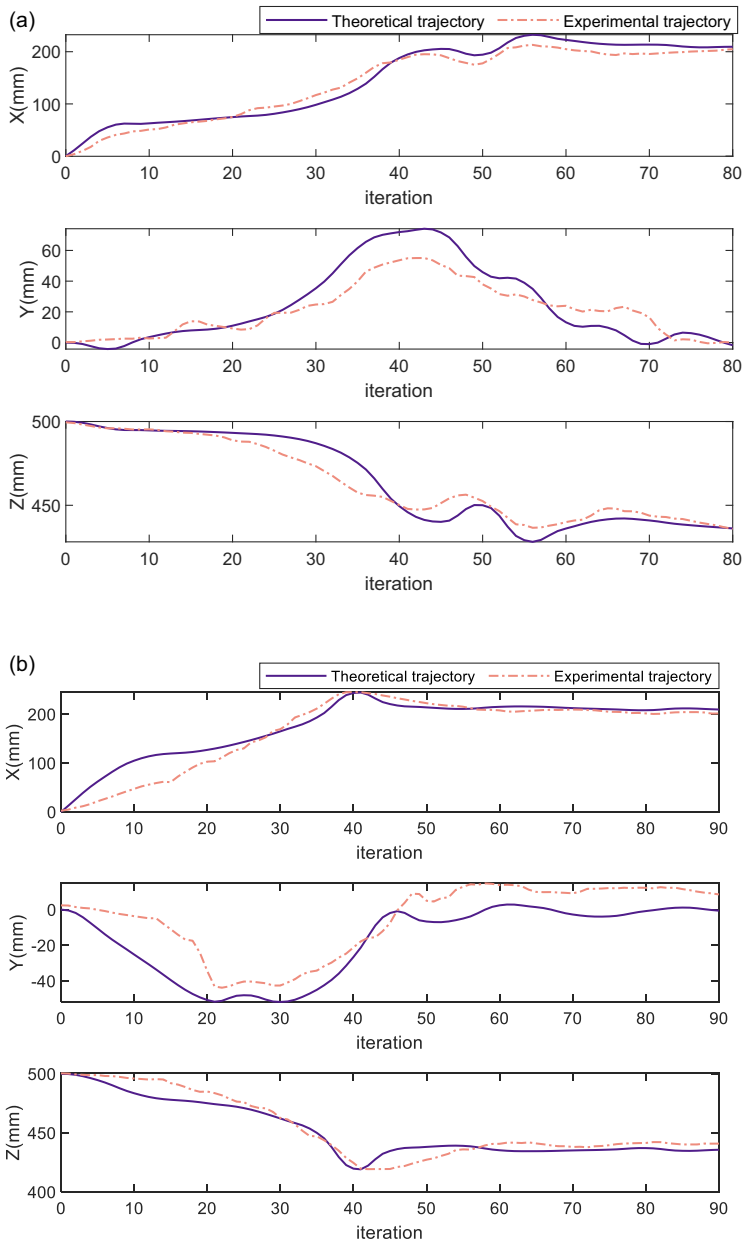


Figure 16. (a) Coordinate curves in the single obstacle environment and (b) coordinate curves in the multi-obstacles environment.

4.2. Experimental verification

The experiment is designed to verify the obstacle avoidance planning effect of the continuum robot by adopting the proposed path planning method. Figure 14 shows the physical prototype platform of a two-segment cable-driven continuum robot. The two planned paths obtained from above simulation are executed by sending the cable length to the controller, and the moving process in two obstacle environments is shown in Fig. 15.

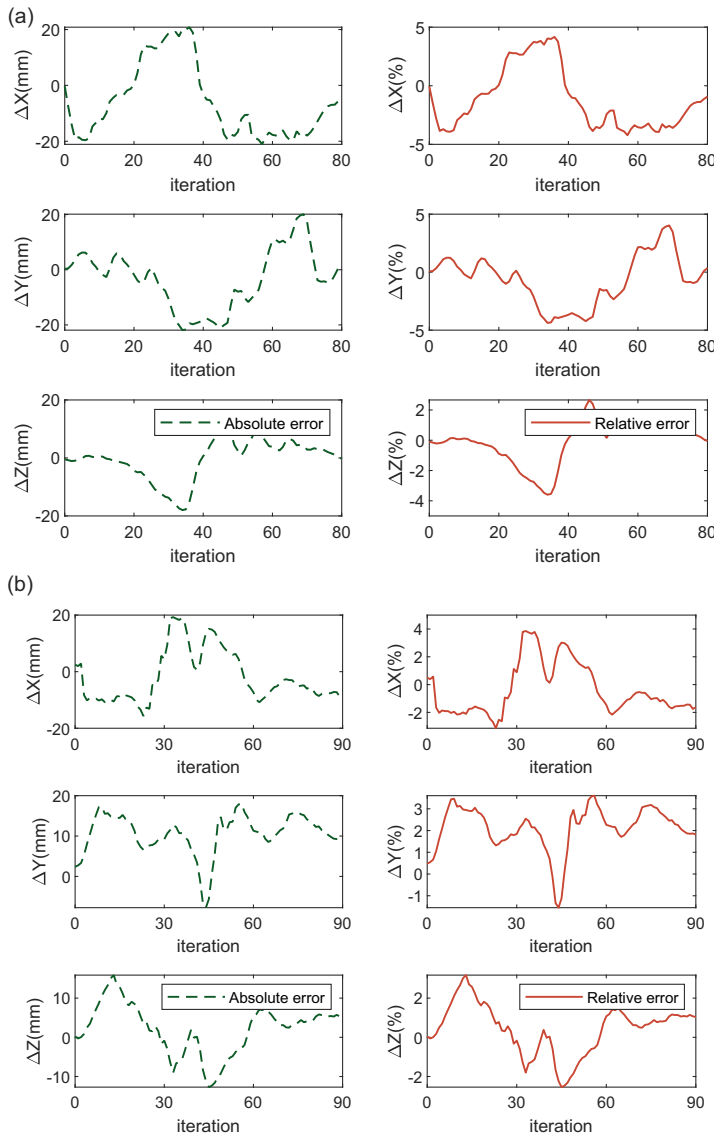


Figure 17. (a) Errors of planned path in the single obstacle environment and (b) errors of planned path in the multi-obstacles environment.

The continuum robot end moved along the desired path and avoided the obstacle well in both the cases. Figure 16 presents the experimental coordinate data of the continuum robot end in the base coordinate frame and Fig. 17 shows the error analysis between theoretical and experimental values. As shown in Fig. 17, the absolute error of each coordinate axis remains within the error band of $[-20, +20]$ mm and the relative error is controlled within 5%. Compared to the ideal simulation, the continuum robot end in its initial vertical state has a certain offset from the base coordinate frame under the influence of gravity. Meanwhile, the prototype lacks a self-calibrating cable length mechanism where some of the actuated cables are slack in the initial motion, resulting in significant errors in the motion process. In addition, possible causes of errors include friction between ropes and holes, deformation of the elastic structures and measurement errors. Overall, the experimental results are in reasonable agreement with the simulation results.

5. Conclusion

In this paper, a novel collision-free path planning method based on BAS-APF algorithm is presented for the continuum robot, which avoids the complex inverse kinematics and solves the local optimum problem. This method searches forward in the configuration space through the antennae's direction vector and utilizes the BAS algorithm to find the attitude angle guided by the decreasing artificial potential field until reaching the target point. Numerical simulation and experimental results on the two-segment cable-driven continuum robot have verified the efficiency of the planning method. Similarly, the proposed path planning method can also extend to continuum robots with other configurations. Further potential direction for improving the path planning performance includes establishing a synchronous planning scheme that takes into account the shape control of the continuum arm while avoiding obstacles and reaching the target. Another aspect to be considered is to further improve the applicability of the algorithm in a dynamic environment with multiple obstacles.

Author contributions. Meng Ding, Jian Guo and Yu Guo conceived and designed the study. Meng Ding and Xianjie Zheng established the experimental platform and conducted experimental verification. Meng Ding, Liaoxue Liu and Yu Guo wrote the article.

Financial support. This research is supported by the National Natural Science Foundation of China (Grant No.61973167).

Competing interests. The authors declare no competing interests exist.

Ethical approval. Not applicable.

References

- [1] M. Russo, S. M. H. Sadati, X. Dong, A. Mohammad, I. D. Walker, C. Bergeles, K. Xu and D. A. Axinte, "Continuum robots: An overview," *Adv. Intell. Syst.* **5**(5), 2200367 (2023).
- [2] C. Armanini, F. Boyer, A. T. Mathew, C. Duriez and F. Renda, "Soft robots modeling: A structured overview," *IEEE Trans. Rob.* **39**(3), 1728–1748 (2023).
- [3] C. D. Santina, C. Duriez and D. Rus, "Model-based control of soft robots: A survey of the state of the art and open challenges," *IEEE Control Syst. Mag.* **43**(3), 30–65 (2023).
- [4] H. Yuan, L. Zhou and W. Xu, "A comprehensive static model of cable-driven multi-section continuum robots considering friction effect," *Mech. Mach. Theory* **135**, 130–149 (2019).
- [5] R. Buckingham and A. Graham, "Nuclear snake-arm robots," *Ind. Robot* **39**(1), 6–11 (2012).
- [6] L. Angrisani, S. Grazioso, G. D. Gironimo, D. Panariello and A. Tedesco, "On the Use of Soft Continuum Robots for Remote Measurement Tasks in Constrained Environments: A Brief Overview of Applications," *IEEE International Symposium on Measurements & Networking (M&N)*, 2019, Catania, Italy (2019) pp. 1–5.
- [7] P. E. Dupont, N. Simaan, H. Choset and C. Rucker, "Continuum robots for medical interventions," *Proc. IEEE* **110**(7), 847–870 (2022).
- [8] X. Hu, A. Chen, Y. Luo, C. Zhang and E. Zhang, "Steerable catheters for minimally invasive surgery: A review and future directions," *Comput. Assist. Surg.* **23**(1), 21–41 (2018).
- [9] Y. Ansari, M. Manti, E. Falotico, M. Cianchetti and C. Laschi, "Multiobjective optimization for stiffness and position control in a soft robot arm module," *IEEE Robot. Autom. Lett.* **3**(1), 108–115 (2017).
- [10] M. M. Tonapi, I. S. Godage, A. M. Vijaykumar and I. D. Walker, "A novel continuum robotic cable aimed at applications in space," *Adv. Robot.* **29**(13), 861–875 (2015).
- [11] J. Peng, W. Xu, T. Liu, H. Yuan and B. Liang, "End-effector pose and armshape synchronous planning methods of a hyper-redundant manipulator for spacecraft repairing," *Mech. Mach. Theory* **155**, 104062 (2021).
- [12] A. H. Memar and K. T. M. Keshmiri, "Motion Planning for a Multi-segment Continuum robot," *Proceedings of the International Conference on Mechanical Engineering and Mechatronics*, Ottawa, Ontario, Canada (2012) pp. 209–1–209–9.
- [13] B. H. Meng, I. S. Godage and I. Kanj, "RRT*-based path planning for pontinuum arms," *IEEE Robot. Autom. Lett.* **7**(3), 6830–6837 (2022).
- [14] J. Lai, B. Lu, Q. Zhao and H. K. Chu, "Constrained motion planning of a cable-driven soft robot with compressible curvature modeling," *IEEE Robot. Autom. Lett.* **7**(2), 4813–4820 (2022).
- [15] G. Niu, Z. Zheng and Q. Gao, "Collision Free Path Planning based on Region Clipping for Aircraft Fuel Tank Inspection Robot," *2014 IEEE International Conference on Robotics and Automation (ICRA)*, 2014, Hong Kong, China (2014) pp. 3227–3233.
- [16] H. Ananthanarayanan and R. Ordóñez, "A fast converging optimal technique applied to path planning of hyper-redundant manipulators," *Mech. Mach. Theory* **118**, 231–246 (2017).

- [17] H. Wang, J. Chen, H. Y. K. Lau and H. Ren, “Motion planning based on learning from demonstration for multiple-segment exible soft robots actuated by electroactive polymers,” *IEEE Robot. Autom. Lett.* **1**(1), 391–398 (2016).
- [18] N. Tan, P. Yu, Z. Zhong and Y. Zhang, “Data-driven control for continuum robots based on discrete zeroing neural networks,” *IEEE Trans. Ind. Inform.* **19**(5), 7088–7098 (2023).
- [19] Z. Mu, Y. Chen, Z. Li, N. D. C. Wang and H. Qian, “A combined planning method based on biarc curve and bézier curve for concentric cable-driven manipulators working in confined environments,” *IEEE/ASME Trans. Mechatron.* **27**(6), 4475–4486 (2022).
- [20] A. Ataka, P. Qi, A. Shiva, A. Shafti, H. Wurdemann, H. Liu and K. Althoefer, “Real-time Pose Estimation and Obstacle Avoidance for Multi-segment Continuum Manipulator in Dynamic Environments,” *2016 IEEE/RSJ International Conference on Intelligent Robots and Systems (IROS)*, 2016, Daejeon, Korea (South) (2012) pp. 2012–2832.
- [21] D. Xu, E. Li, R. Guo, J. Liu and Z. Liang, “A cable-driven hyperredundant manipulator: Obstacle-avoidance path planning and tension optimization,” *IEEE Robot. Autom. Mag.* **29**(3), 107–126 (2022).
- [22] Y. Tian, X. Zhu, D. Meng, X. Wang and B. Liang, “An overall configuration planning method of continuum hyper-redundant manipulators based on improved artificial potential field method,” *IEEE Robot. Autom. Lett.* **6**(3), 4867–4874 (2021).
- [23] A. Mohammad, M. Russo, Y. Fang, X. Dong, D. Axinte and J. Kell, “An efficient follow-the-leader strategy for continuum robot navigation and coiling,” *IEEE Robot. Autom. Lett.* **6**(4), 7493–7500 (2021).
- [24] E. Amanov, T.-D. Nguyen and J. Burgner-Kahrs, “Tendon-driven continuum robots with extensible sections—A model-based evaluation of path-following motions,” *Int. J. Robot. Res.* **240**(1), 7–23 (2021).
- [25] T. Liu, W. Xu, T. Yang and Y. Li, “A hybrid active and passive cable-driven segmented redundant manipulator: Design, kinematics, and planning,” *IEEE/ASME Trans. Mechatron.* **26**(2), 930–942 (2021).
- [26] A. Parvaresh and S. Moosavian, “Dynamics and path tracking of continuum robotic arms using data-driven identification tools,” *Robotica* **40**(4), 1098–1124 (2022).
- [27] P. Niu, L. Han, Y. Huang and L. Yan, “Shape-controllable inverse kinematics of hyper-redundant robots based on the improved FABRIK method,” *Robotica* **42**(1), 225–241 (2024). doi: [10.1017/S0263574723001455](https://doi.org/10.1017/S0263574723001455).
- [28] Z. Pan, D. Li, K. Yang and H. Deng, “Multi-robot obstacle avoidance based on the improved artificial potential field and PID adaptive tracking control algorithm,” *Robotica* **37**(11), 1883–1903 (2019).
- [29] Z. He, X. Chu, C. Liu and W. Wu, “A novel model predictive artificial potential field based ship motion planning method considering colregs for complex encounter scenarios,” *ISA Trans.* **134**, 58–73 (2023).
- [30] X. Jiang and S. Li, “BAS: Beetle antennae search algorithm for optimization problems,” *Int. J. Robot. Control* **1**(1), 1–5 (2018).
- [31] Y. Zhang, S. Li and B. Xu, “Convergence analysis of beetle antennae search algorithm and its applications,” *Soft Comput.* **25**(16), 10595–10608 (2021).
- [32] Q. Wu, H. Lin, Y. Jin, Z. Chen and D. Chen, “A new fallback beetle antennae search algorithm for path planning of mobile robots with collision-free capability,” *Soft Comput.* **24**(15), 2369–2380 (2020).
- [33] A. H. Khan, S. Li and X. Luo, “Obstacle avoidance and tracking control of redundant robotic manipulator: An RNN-based metaheuristic approach,” *IEEE Trans. Ind. Inform.* **16**(7), 4670–4680 (2020).
- [34] A. T. Khan, S. Li and X. Zhou, “Trajectory optimization of 5-link biped robot using beetle antennae search,” *IEEE Trans. Circuits Syst. II Express Briefs* **68**(10), 3276–3280 (2021).
- [35] D. Chen, X. Li and S. Li, “A novel convolutional neural network model based on beetle antennae search optimization algorithm for computerized tomography diagnosis,” *IEEE Trans. Neural Netw. Learn. Syst.* **34**(3), 1418–1429 (2023).
- [36] X. Li, H. Jiang, M. Niu and R. Wang, “An enhanced selective ensemble deep learning method for rolling bearing fault diagnosis with beetle antennae search algorithm,” *Mech. Syst. Signal Process* **142**, 106752 (2020).
- [37] Q. Huang, L. Xie, G. Yin, M. Ran, X. Liu and J. Zheng, “Acoustic signal analysis for detecting defects inside an arc magnet using a combination of variational mode decomposition and beetle antennae search,” *ISA Trans.* **102**, 347–364 (2020).
- [38] X. Zheng, M. Ding, L. Liu, Y. Zhu and Y. Guo, “Static-to-kinematic modeling and experimental validation of tendon-driven quasi continuum manipulators with nonconstant subsegment stiffness,” *Chin. Phys. B* **33**(1), 010703 (2024). doi: [10.1088/1674-1056/acfaf8](https://doi.org/10.1088/1674-1056/acfaf8).
- [39] R. Webster and B. A. Jones, “Design and kinematic modeling of constant curvature continuum robots: A review,” *Int. J. Robot. Res.* **29**(13), 1661–1683 (2010).
- [40] R. Menasri, A. Nakib, B. Daachi, H. Oulhadj and P. Siarry, “A trajectory planning of redundant manipulators based on bilevel optimization,” *Appl. Math. Comput.* **250**, 934–947 (2015).
- [41] R. Tomasz, W. Mateusz and L. B. Fatina, “Optimal collision-free path planning of a free-floating space robot using spline-based trajectories,” *Acta Astronaut.* **190**, 395–408 (2022).